

Fundamental limits on the rate of bacterial cell division

³ **Nathan M. Belliveau^{†, 1}, Griffin Chure^{†, 2, 3}, Christina L. Hueschen⁴, Hernan G.**
⁴ **Garcia⁵, Jané Kondev⁶, Daniel S. Fisher⁷, Julie Theriot^{1, 8}, Rob Phillips^{2, 9, *}**

*For correspondence:

¹These authors contributed equally
to this work

⁵ Department of Biology, University of Washington, Seattle, WA, USA; ²Division of Biology
and Biological Engineering, California Institute of Technology, Pasadena, CA, USA;
⁷ Department of Applied Physics, California Institute of Technology, Pasadena, CA, USA;
⁸ Department of Chemical Engineering, Stanford University, Stanford, CA, USA;
⁹ Department of Molecular Cell Biology and Department of Physics, University of
California Berkeley, Berkeley, CA, USA; ⁶Department of Physics, Brandeis University,
¹¹ Waltham, MA, USA; ⁷Department of Applied Physics, Stanford University, Stanford, CA,
¹² USA; ⁸Allen Institute for Cell Science, Seattle, WA, USA; ⁹Department of Physics, California
¹³ Institute of Technology, Pasadena, CA, USA; *Contributed equally

14

¹⁵ **Abstract** This will be written next

16

17 Uptake of Nutrients

18 In order to build new cellular mass, the molecular and elemental building blocks must be scavenged
 19 from the environment in different forms. Carbon, for example, is acquired via the transport of
 20 carbohydrates and sugar alcohols with some carbon sources receiving preferential treatment
 21 in their consumption (*Monod, 1947*). Phosphorus, sulfur, and nitrogen, on the other hand, are
 22 harvested primarily in the forms of inorganic salts, namely phosphate, sulfate, and ammonia
 23 (*Jun et al., 2018; Assentoft et al., 2016; Stasi et al., 2019; Antonenko et al., 1997; Rosenberg et al.,*
 24 *1977; Willsky et al., 1973*). All of these compounds have different permeabilities across the cell
 25 membrane and most require some energetic investment either via ATP hydrolysis or through the
 26 proton electrochemical gradient to bring the material across the hydrophobic cell membrane. Given
 27 the diversity of biological transport mechanisms and the vast number of inputs needed to build a
 28 cell, we begin by considering transport of some of the most important cellular ingredients: carbon,
 29 nitrogen, oxygen, hydrogen, phosphorus, and sulfur.

30 The elemental composition of *E. coli* has received much quantitative attention over the past
 31 half century (*Neidhardt et al., 1991; Taymaz-Nikerel et al., 2010; Heldal et al., 1985; Bauer and Ziv,*
 32 *1976*), providing us with a starting point for estimating the copy numbers of various transporters.
 33 While there is some variability in the exact elemental percentages (with different uncertainties), we
 34 can estimate that the dry mass of a typical *E. coli* cell is \approx 45% carbon (BNID: 100649, *Milo et al.*
 35 (*2010*)), \approx 15% nitrogen (BNID: 106666, *Milo et al. (2010)*), \approx 3% phosphorus (BNID: 100653, *Milo*
 36 *et al. (2010)*), and 1% sulfur (BNID: 100655, *Milo et al. (2010)*). In the coming paragraphs, we will
 37 engage in a dialogue between back-of-the-envelope estimates for the numbers of transporters
 38 needed to facilitate these chemical stoichiometries and the experimental proteomic measurements
 39 of the biological reality. Such an approach provides the opportunity to test if our biological knowl-
 40 edge is sufficient to understand the scale at which these complexes are produced. Specifically, we
 41 will make these estimates considering a modest doubling time of 5000 s, a growth rate of \approx 0.5 hr⁻¹,

42 the range in which the majority of the experimental measurements reside.

43 **Nitrogen Transport**

44 Before we begin our back-of-the-envelope estimations, we must address which elemental sources
 45 must require proteinaceous transport, meaning that the cell cannot acquire appreciable amounts
 46 simply via diffusion from the membrane. The permeability of the lipid membrane to a large
 47 number of solutes has been extensively characterized over the past century. Large, polar molecular
 48 species (such as various sugar molecules, sulfate, and phosphate) have low permeabilities while
 49 small, non-polar compounds (such as oxygen, carbon dioxide, and ammonia) can readily diffuse
 50 across the membrane. Ammonia, a primary source of nitrogen in typical laboratory conditions,
 51 has a permeability on par with water ($\approx 10^5$ nm/s, BNID:110824 *Milo et al. (2010)*). In particularly
 52 nitrogen-poor conditions, *E. coli* expresses a transporter (AmtB) which appears to aid in nitrogen
 53 assimilation, though the mechanism and kinetic details of transport is still a matter of debate (*van*
 54 *Heeswijk et al., 2013; Khademi et al., 2004*). Beyond ammonia, another plentiful source of nitrogen
 55 come in the form of glutamate, which has its own complex metabolism and scavenging pathways.
 56 However, nitrogen is plentiful in the growth conditions examined in this work, permitting us to
 57 neglect nitrogen transport as a potential rate limiting process in cell division in typical experimental
 58 conditions. We direct the reader to the supplemental information for a more in-depth discussion of
 59 permeabilities and a series of calculations revealing that active nitrogen transport can be neglected
 60 for the purposes of this article.

61 **Carbon Transport**

62 We begin our estimations with the most abundant element in *E. coli* by mass, carbon. Using
 63 ≈ 0.3 pg as the typical *E. coli* dry mass (BNID: 103904, *Milo et al. (2010)*), we estimate that \approx
 64 10^{10} carbon atoms must be brought into the cell in order to double all of the carbon-containing
 65 molecules (*Figure 1(A, top)*). Typical laboratory growth conditions, such as those explored in the
 66 aforementioned proteomic data sets, provide carbon as a single class of sugar such as glucose,
 67 galactose, or xylose to name a few. *E. coli* has evolved myriad mechanisms by which these sugars can
 68 be transported across the cell membrane. One such mechanism of transport is via the PTS system
 69 which is a highly modular system capable of transporting a diverse range of sugars (*Escalante*
 70 *et al., 2012*). The glucose-specific component of this system transports ≈ 200 glucose molecules
 71 per second per channel (BNID: 114686, *Milo et al. (2010)*). Making the assumption that this is a
 72 typical sugar transport rate, coupled with the need to transport 10^{10} carbon atoms, we arrive at the
 73 conclusion that on the order of 1,000 transporters must be expressed in order to bring in enough
 74 carbon atoms to divide in 5000 s, diagrammed in the top panel of *Figure 1(A)*. This estimate, along
 75 with the observed average number of the PTS system carbohydrate transporters present in the
 76 proteomic data sets (*Schmidt et al., 2016; Peebo et al., 2015; Valgepea et al., 2013; Li et al., 2014*),
 77 is shown in *Figure 1(A)*. While we estimate 1500 transporters are needed with a 5000 s division
 78 time, we can abstract this calculation to consider any particular growth rate given knowledge of
 79 the cell density and volume as a function of growth rate and direct the reader to the SI for more
 80 information. As revealed in *Figure 1(A)*, experimental measurements exceed the estimate by several
 81 fold, illustrating that transport of carbon in to the cell is not rate limiting for cell division.

82 The estimate presented in *Figure 1(A)* neglects any specifics of the regulation of carbon transport
 83 system and presents a data-averaged view of how many carbohydrate transporters are present
 84 on average. Using the diverse array of growth conditions explored in the proteomic data sets, we
 85 can explore how individual carbon transport systems depend on the population growth rate. In
 86 *Figure 1(B)*, we show the total number of carbohydrate transporters specific to different carbon
 87 sources. A striking observation, shown in the top-left plot of *Figure 1(B)*, is the constancy in the
 88 expression of the glucose-specific transport systems. Additionally, we note that the total number
 89 of glucose-specific transporters is tightly distributed $\approx 10^4$ per cell, the approximate number of
 90 transporters needed to sustain rapid growth of several divisions per hour, as indicated by the grey

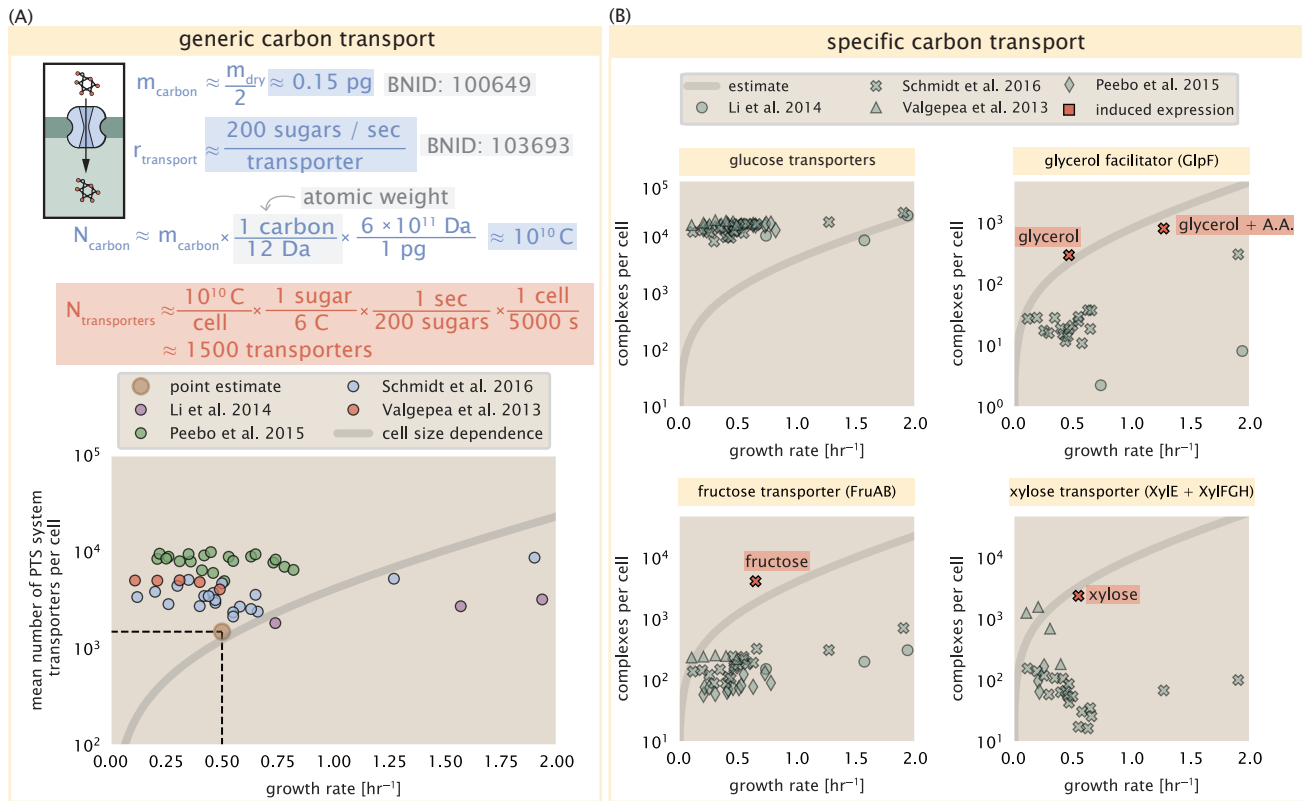


Figure 1. The abundance of carbon transport systems across growth rates. (A) A simple estimate for the minimum number of generic carbohydrate transport systems (top) assumes $\approx 10^{10}$ C are needed to complete division, each transported sugar contains ≈ 6 C, and each transporter conducts sugar molecules at a rate of ≈ 200 per second. Bottom plot shows the estimated number of transporters needed at a growth rate of ≈ 0.5 per hr (light-brown point and dashed lines). Colored points correspond to the mean number of PTS system sugar transporters (complexes annotated with the Gene Ontology term GO:0009401) for different growth conditions across different published datasets. (B) The abundance of various specific carbon transport systems plotted as a function of the population growth rate. Red points and red-highlighted text indicate conditions in which the only source of carbon in the growth medium induces expression of the transport system. Grey line in (A) and (B) represents the estimated number of transporters per cell at a continuum of growth rates.

shaded line. This illustrates that *E. coli* maintains a substantial number of complexes present for transporting glucose which is known to be the preferential carbon source (*Monod, 1947; Liu et al., 2005; Aidelberg et al., 2014*).

It is now understood that a large number of metabolic operons are regulated with dual-input logic gates that are only expressed when glucose concentrations are low (mediated by cyclic-AMP receptor protein CRP) and the concentration of other carbon sources are elevated (*Gama-Castro et al., 2016; Zhang et al., 2014b*). A famed example of such dual-input regulatory logic is in the regulation of the *lac* operon which is only natively activated in the absence of glucose and the presence of allolactose, an intermediate in lactose metabolism (*Jacob and Monod, 1961*), though we now know of many other such examples (*Ireland et al., 2020; Gama-Castro et al., 2016; Belliveau et al., 2018*). This illustrates that once glucose is depleted from the environment, cells have a means to dramatically increase the abundance of the specific transporter needed to digest the next sugar that is present. Several examples of induced expression of specific carbon-source transporters are shown in *Figure 1(B)*. Points colored in red (labeled by red text-boxes) correspond to growth conditions in which the specific carbon source (glycerol, xylose, or fructose) is present. These plots show that, in the absence of the particular carbon source, expression of the transporters is maintained on the order of $\sim 10^2$ per cell. However, when induced, the transporters become highly-expressed and fall close to the predicted number of transporters needed to facilitate growth on that substrate alone, shown as a transparent grey line. Together, this generic estimation and the specific examples of induced expression suggest that transport of carbon across the cell membrane, while critical for growth, is not the rate-limiting step of cell division.

112 Phosphorus and Sulfur Transport

We now turn our attention towards other essential elements, namely phosphorus and sulfur. Phosphorus is critical to the cellular energy economy in the form of high-energy phosphodiester bonds making up DNA, RNA, and the NTP energy pool as well as playing a critical role in the post-translational modification of proteins and defining the polar-heads of lipids. In total, phosphorus makes up $\approx 3\%$ of the cellular dry mass which in typical experimental conditions is in the form of inorganic phosphate. The cell membrane has remarkably low permeability to this highly-charged and critical molecule, therefore requiring the expression of active transport systems. In *E. coli*, the proton electrochemical gradient across the inner membrane is leveraged to transport inorganic phosphate into the cell (*Rosenberg et al., 1977*). Proton-solute symporters are widespread in *E. coli* (*Ramos and Kaback, 1977; Booth et al., 1979*) and can have rapid transport rates of 50 to 100 molecules per second for sugars and other solutes (BNID: 103159; 111777, *Milo et al. (2010)*). As a more extreme example, the proton transporters in the F₁-F₀ ATP synthase, which leverage the proton electrochemical gradient for rotational motion, can shuttle protons across the membrane at a rate of ≈ 1000 per second (BNID: 104890; 103390, *(Milo et al., 2010)*). In *E. coli* the PitA phosphate transport system has been shown to very tightly coupled with the proton electrochemical gradient with a 1:1 proton:phosphate stoichiometric ratio (*Harris et al., 2001; Feist et al., 2007*). Taking the geometric mean of the aforementioned estimates gives a plausible rate of phosphate transport on the order of 300 per second. Illustrated in *Figure 2(A)*, we can estimate that ≈ 150 phosphate transporters are necessary to maintain an $\approx 3\%$ dry mass with a 5000 s division time. This estimate is again satisfied when we examine the observed copy numbers of PitA in proteomic data sets (plot in *Figure 2(A)*). While our estimate is very much in line with the observed numbers, we emphasize that this is likely a slight over estimate of the number of transporters needed as there are other phosphorous scavenging systems, such as the ATP-dependent phosphate transporter Pst system which we have neglected.

Satisfied that there are a sufficient number of phosphate transporters present in the cell, we now turn to sulfur transport as another potentially rate limiting process. Similar to phosphate, sulfate is highly-charged and not particularly membrane permeable, requiring active transport. While there exists a H⁺/sulfate symporter in *E. coli*, it is in relatively low abundance and is not well

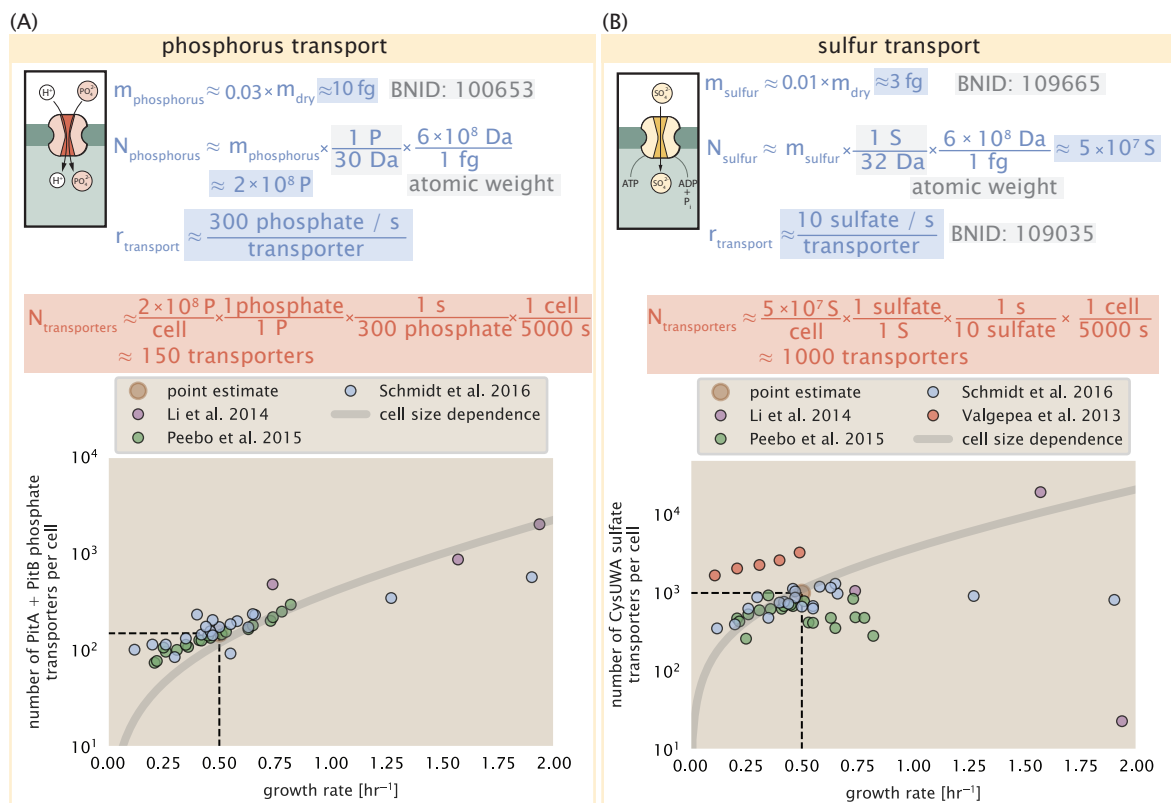


Figure 2. Estimates and measurements of phosphate and sulfate transport systems as a function of growth rate. (A) Estimate for the number of PitA phosphate transport systems needed to maintain a 3% phosphorus *E. coli* dry mass. Points in plot correspond to the total number of PitA transporters per cell. (B) Estimate of the number of CysUWA complexes necessary to maintain a 1% sulfur *E. coli* dry mass. Points in plot correspond to average number of CysUWA transporter complexes that can be formed given the transporter stoichiometry [CysA]₂[CysU][CysW][Sbp/CysP]. Grey line in (A) and (B) represents the estimated number of transporters per cell at a continuum of growth rates.

characterized (Zhang et al., 2014a). Sulfate is predominantly acquired via the ATP-dependent ABC transporter CysUWA system which also plays an important role in selenium transport (Sekowska et al., 2000; Sirko et al., 1995). While specific kinetic details of this transport system are not readily available, generic ATP transport systems in prokaryotes transport on the order of 1 to 10 molecules per second (BNID: 109035, Milo et al. (2010)). Combining this generic transport rate, measurement of sulfur comprising 1% of dry mass, and a 5000 second division time yields an estimate of ≈ 1000 CysUWA complexes per cell (Figure 2(B)). Once again, this estimate is in notable agreement with proteomic data sets, suggesting that there are sufficient transporters present to acquire the necessary sulfur. In a similar spirit of our estimate of phosphorus transport, we emphasize that this is likely an overestimate of the number of necessary transporters as we have neglected other sulfur scavenging systems that are in lower abundance.

152 Limits on Transporter Expression

So which, if any, of these processes may be rate limiting for growth? As suggested by ?? (B), induced expression can lead to an order-of-magnitude (or more) increase in the amount of transporters needed to facilitate transport. Thus, if acquisition of nutrients was the limiting state in cell division, could expression simply be increased to accommodate faster growth? A way to approach this question is to compute the amount of space in the bacterial membrane that could be occupied by nutrient transporters. Considering a rule-of-thumb for the surface area of *E. coli* of about 6 μm^2 (BNID: 101792, Milo et al. (2010)), we expect an areal density for 1000 transporters to be approximately 200 transporters/ μm^2 . For a typical transporter occupying about 50 nm²/dimer, this

amounts to about only 1 percent of the total inner membrane (*Szenk et al., 2017*). In addition, bacterial cell membranes typically have densities of 10^5 proteins/ μm^2 (*Phillips, 2018*), implying that the cell could accommodate more transporters of a variety of species if it were rate limiting. As we will see in the next section, however, occupancy of the membrane can impose other limits on the rate of energy production.

166 Protein synthesis

167 Lastly, we turn our attention to the process of translation. So far our estimates have led to protein
 168 copy numbers that are consistent with the proteomic data, or even in excess of what might be
 169 needed for each task under limiting growth conditions. Even in our example of *E. coli* grown under
 170 different carbohydrate sources (*Figure 1(B)*), cells can utilize alternative carbon sources by inducing
 171 the expression of additional membrane transporters and enzymes. Optimal resource allocation
 172 and the role of ribosomal proteins have been an area of intense quantitative study over the last
 173 decade by Hwa and others (*Scott et al., 2010; Hui et al., 2015*). From the perspective of limiting
 174 growth, our earlier estimate of rRNA highlighted the necessity for multiple copies of rRNA genes in
 175 order to make enough rRNA, suggesting the possibility that synthesis of ribosomes might be rate
 176 limiting. While the transcriptional demand for the ribosomal proteins is substantially lower than
 177 rRNA genes, since many proteins can be translated from relatively fewer mRNA, other ribosomal
 178 proteins like the translation elongation factor EF-Tu also present a substantial burden. For EF-Tu in
 179 particular, it is the most highly expressed protein in *E. coli* and is expressed by multiple genes on
 180 the chromosome, *tufA* and *tufB*.

181 We can begin to gain some intuition into how translation might limit growth by noting that the
 182 total number of peptide bonds generated as the cell doubles, N_{aa} , will be given by, $\tau \cdot r_t \cdot R / \ln(2)$.
 183 Here, τ refers to the doubling time of the cell under steady-state growth and the factor $\ln(2)$ is due
 184 to exponential growth. r_t is the maximum translation elongation rate, and R is the average number
 185 of ribosomes per cell. With the growth rate related to the cell doubling time by $\lambda = \ln(2)/\tau$, we can
 186 write the translation-limited growth rate as,

$$\lambda_{\text{translation-limited}} = \frac{r_t \cdot R}{N_{aa}}. \quad (1)$$

187 Alternatively, since N_{aa} is related to the total protein mass through the molecular weight of each
 188 protein, we can also consider the growth rate in terms of ribosomal mass fraction. By making the
 189 approximation that an average amino acid has a molecular weight of 110 Da (see *Figure 3(A)*), we
 190 can rewrite the growth rate as,

$$\lambda_{\text{translation-limited}} \approx \frac{r_t}{L_R} \Phi_R, \quad (2)$$

191 where L_R is the total length in amino acids that make up a ribosome, and Φ_R is the ribosomal
 192 mass fraction. This is plotted as a function of ribosomal fraction Φ_R in *Figure 3(A)*, where we take
 193 $L_R \approx 7459$ aa, corresponding to the length in amino acids for all ribosomal subunits of the 50S
 194 and 30S complex (BNID: 101175, (*Milo et al., 2010*)). This formulation assumes that the cell can
 195 transcribe the required amount of rRNA, which appears reasonable for *E. coli* under the allowing us
 196 to consider the inherent limit on growth set by the ribosome.

197 The growth rate defined by Equation 2 reflects mass-balance under steady-state growth and
 198 has long provided a rationalization to the apparent linear increase in *E. coli*'s ribosomal content
 199 as a function of growth rate (*Maaløe, 1979; Scott et al., 2010*). For our purposes, there are several
 200 important consequences of this trend. Perhaps the first thing to notice is that there is a maximum
 201 growth rate at about $\lambda \approx 6\text{hr}^{-1}$, or doubling time of about 7 minutes (dashed line). This growth rate
 202 can be viewed as an inherent maximum growth rate due to the need for the cell to double the cell's
 203 entire ribosomal mass. Interestingly, this limit is independent of the absolute number of ribosomes,
 204 but rather is simply given by time to translate an entire ribosome, L_R/r_t . As shown in *Figure 3(B)*, we

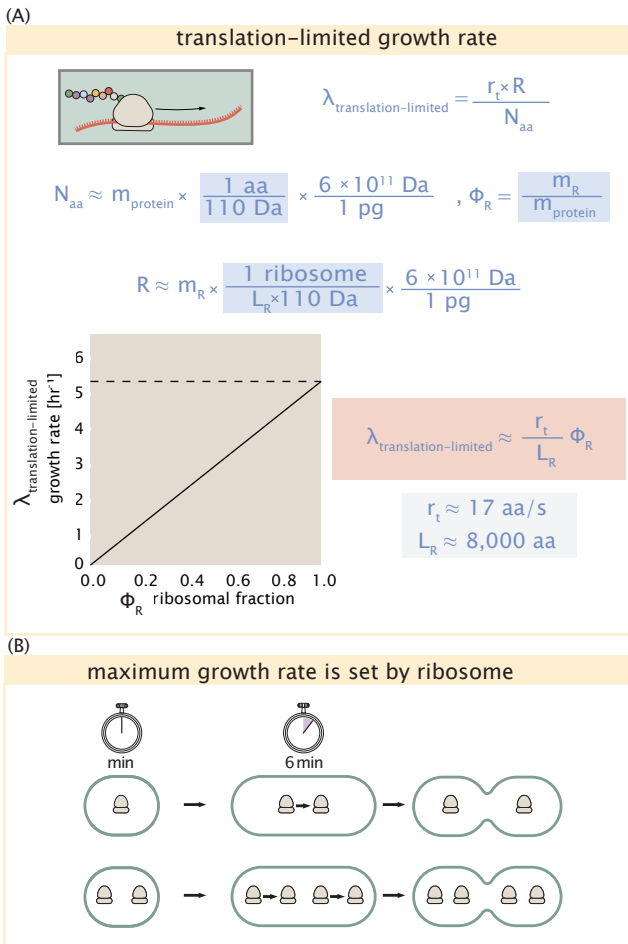


Figure 3. Translation-limited growth rate. (A) Here we consider the translation-limited growth as a function of ribosomal fraction. By mass balance, the time required to double the entire proteome (N_{aa} / r_t) sets the translation-limited growth rate, $\lambda_{\text{translation-limited}}$. Here N_{aa} is effectively the number of peptide bonds that must be translated, r_t is the translation elongation rate, and R is the number of ribosomes. This can also be re-written in terms of the ribosomal mass fraction $\Phi_R = m_R / m_{\text{protein}}$, where m_R is the total ribosomal mass and m_{protein} is the mass of all proteins in the cell. L_R refers to the summed length of the ribosome in amino acids. $\lambda_{\text{translation-limited}}$ is plotted as a function of Φ_R (solid line). (B) The dashed line in part (A) identifies a maximum growth rate that is set by the ribosome. Specifically, this growth rate corresponds to the time required to translate an entire ribosome, L_R / r_t . This is a result that is independent of the number of ribosomes in the cell as shown schematically here.

205 can reconcile this with the observation that in order to double the average number of ribosomes,
206 each ribosome must produce a second ribosome. This is a process that cannot be parallelized.

207 For reasonable values of Φ_R , between about 0.1 - 0.3 (Scott et al., 2010), the maximum growth
208 rate is in line with experimentally reported growth rates around 0.5 - 2 hr^{-1} . Here we are implicitly
209 assuming that translation proceeds randomly, without preference between ribosomal or non-
210 ribosomal mRNA, which appears reasonable. Importantly, in order for a cell to scale this growth
211 limit set by Φ_R , cells *must* increase their ribosomal abundance. This can be achieved by either
212 synthesizing more ribosomes or reducing the fraction of non-ribosomal proteins. Reduction of
213 non-ribosomal proteins is not straight forward since, as we have found throughout our estimates,
214 doubling a cell requires many other enzymes and transporters. Increasing the absolute ribosomal
215 abundance for the case of *E. coli* is limited by the number of rRNA operons.

216 **Multiple replication forks bias ribosome abundance.**

217 *E. coli* cells grow by an adder mechanism, whereby cells add a constant volume with each cell
218 division (Taheri-Araghi et al., 2015). In conjunction with this, additional rounds of DNA replication
219 are triggered when cells reach a critical volume per origin of replication (Figure 4(A)). This leads to

the classically-described exponential increase in cell size with growth rate *Schaechter et al. (1958)*; *Si et al. (2017, 2019)*. The mechanism behind growth rate control however, has remained elusive. In the context of maximizing growth rate, it is notable that the majority of ribosomal proteins and rRNA operons are found closer to the DNA origin. Given the need to increase to total gene dosage of rRNA operons at faster growth rates, and the intimate relationship between ribosomal content and growth rate we considered above, this raises the possibility that the observed size scaling and increase in chromosomal content might simply be a means for the cell to tune biosynthesis according to its physiological state.

While an increase in transcription has been observed for genes near the origin in rapidly growing *E. coli* (*Scholz et al., 2019*), we were unaware of such characterization at the proteomic level. In order to test whether there is a relative increase in protein expression for genes closer to the origin, we calculated a running boxcar average of protein copy number as a function of each gene's transcriptional start site. While absolute protein copy numbers can vary substantially across the chromosome, we indeed observe a bias in expression under fast growth conditions (*Figure 4(B)*), showing the result using a 0.5 kb averaging window). The dramatic change in protein copy number near the origin mainly reflects the increase in ribosomal protein expression. This trend is in contrast to slower growth conditions where the average copy number is more uniform across the length of the chromosome.

If ribosomal genes (rRNA and ribosomal proteins) are being synthesized according to their available gene dosage we can make two related hypotheses about how their abundance should vary with chromosomal content. The first is that the ribosomal protein fraction should increase in proportion to the average ratio of DNA origins to DNA termini ($\langle \# \text{ ori} \rangle / \langle \# \text{ ter} \rangle$ ratio). This is a consequence of the skew in DNA dosage as cells grow faster. The second is that the absolute number of ribosomes should increase linearly with the number of DNA origins ($\langle \# \text{ ori} \rangle$), since this will reflect the total gene dosage at a particular growth condition.

In order to test each of these expectations we considered the experimental data from *Si et al. (2017)*, which inferred these parameters for cells under nutrient-limited growth. $\langle \# \text{ ori} \rangle / \langle \# \text{ ter} \rangle$ ratio depends on how quickly chromosomes are replicated relative the cell's doubling time τ and is given by $2^{\tau_C/\tau}$. Here τ_C is the time taken to replicate *E. coli*'s chromosome, referred to as the C period of cell division. In *Figure 4(C)* we plot τ_C versus τ that were measured, with data points in red corresponding to *E. coli* strain MG1655, and blue to strain NCM3722. In their work they also measured the total RNA to protein ratio which reflects ribosomal abundance and we show that data along with other recent measurements from *Dai et al.* Indeed we find that the ribosomal fraction increases with $\langle \# \text{ ori} \rangle / \langle \# \text{ ter} \rangle$ (*Figure 4(C)*). We note a systematic difference in the relative abundances from *Peebo et al.* and *Valgepea et al.* that was inconsistent with a number of other measurements of total RNA-to-protein ratios ($\approx \Phi_R \times 2.1$ *Dai et al. (2016)*) and only show the data from *Schmidt et al.* and *Li et al.* for relative ribosome abundances (see supplemental section XX for a more complete discussion).

We can similarly estimate $\langle \# \text{ ori} \rangle$, which depends on how often replication forks are initiated per cell cycle. This is given by the number of overlapping cell cycles, $2^{\tau_{\text{cyc}}/\tau}$, where τ_{cyc} refers to the total time of chromosome replication and cell division. *Figure 4(E)* shows the associated data from *Si et al.*, which we use to estimate $\langle \# \text{ ori} \rangle$ for each growth condition of the proteomic data. In agreement with our expectations, we find a strong correlation between the ribosome copy number and estimated $\langle \# \text{ ori} \rangle$ (*Figure 4(F)*).

These results may also shed some light on the notable increase in ribosomal content that is observed when sublethal doses of antibiotics. Specifically, if rRNA synthesis is rate limiting, and nutrient conditions largely dictate the extent of overlapping DNA replication cycles, than addition of antibiotic will lengthen the doubling time and allow an increase in the abundance of rRNA that can be synthesized over a division cycle. In Supplemental Section XX we consider this further using additional data from *Si et al. (2017)*.

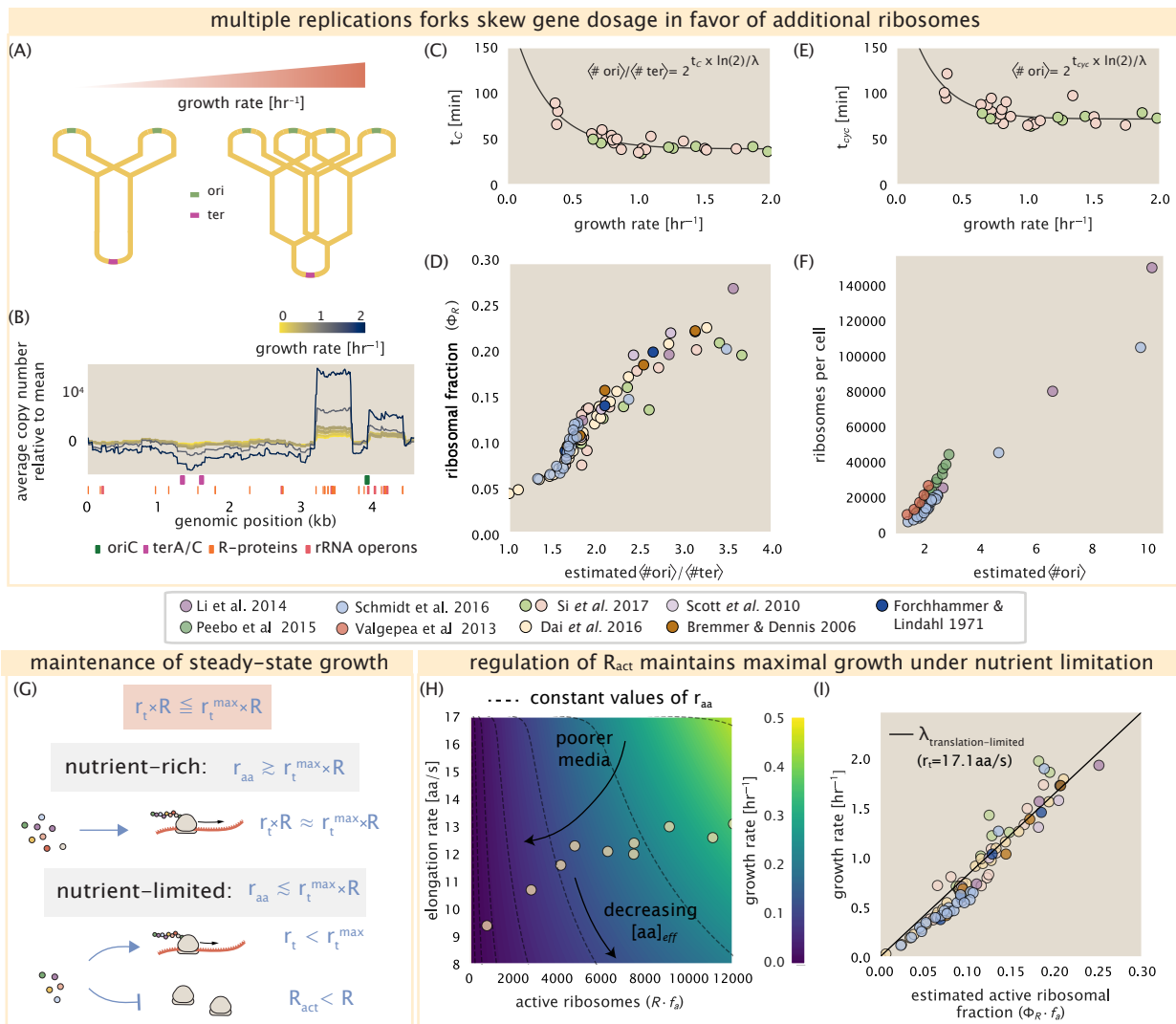


Figure 4. Multiple replication forks skew gene dosage and ribosomal content. (A) Schematic shows the expected increase in replication forks (or number of ori regions) as *E. coli* cells grow faster. (B) A running boxcar average of protein copy number is calculated for each growth condition considered by Schmidt et al.. A 0.5 kb averaging window was used. Protein copy numbers are reported relative to their condition-specific means in order to center all data sets. (C) and (E) show experimental data from Si et al. (2017) Solid lines show fits to the data, which were used to estimate $\langle \# \text{ori} \rangle / \langle \# \text{ter} \rangle$ and $\langle \# \text{ori} \rangle$ [NB: to note fit equations]. Red data points correspond to measurements in strain MG1655, while light green points are for strain NCM3722. (D) Plot compares our estimate of $\langle \# \text{ori} \rangle / \langle \# \text{ter} \rangle$ to the experimental measurements of ribosomal abundance. Ribosomal fraction was approximated from the RNA/protein ratios of Dai et al. (2016) (yellow) and Si et al. (2017) (light red and light green) by the conversion $\Phi_R \approx \Phi_R \cdot 2.1$. (F) plots the ribosome copy number estimated from the proteomic data against our estimate of $\langle \# \text{ori} \rangle$. (G) Schematic showing translation-specific requirements for maintenance of steady-state growth. In a nutrient rich environment, amino acid supply r_{aa} is sufficiently in excess of demand by ribosomes translating at their maximal rate. In poorer nutrient conditions, reduced amino acid supply r_{aa} will decrease the rate of elongation. In a regime where r_{aa} is less than $r_t \cdot R$, the number of actively translating ribosomes will need to be reduced in order to maintain steady-state growth. (H) [in progress], (I) Experimental data from Dai et al. are used to estimate the fraction of actively translating ribosomes. The solid line represents the translation-limited growth rate for ribosomes elongating at 17.1 aa/s.

270 **Regulation of translating ribosomes helps maintain maximal growth according to
271 nutrient availability.**

272 While the above analysis provides an explanation for how *E. coli* appears to vary its ribosomal
273 content to maximize growth, it also presents a challenge in the limit of poorer nutrient conditions.
274 Recall from Equation 2 that ribosomal content should decrease to zero as growth decreases to zero.
275 While bacteria tend to decrease their ribosomal abundance in poorer nutrient conditions, they
276 do so only to some fixed, non-zero amount (*Scott et al., 2010; Liebermeister et al., 2014*). Here
277 we find a minimal ribosomal fraction of about 6 percent in the slowest growth conditions. From
278 the perspective of a bacterium dealing with uncertain nutrient conditions, there is likely a benefit
279 for the cell to maintain some relative fraction of ribosomes to support rapid growth as nutrient
280 conditions improve.

281 The challenge however, lies in the cell's ability to maintain steady-state growth when ribosomes are
282 in excess of the rate that nutrients can be harvested and amino acids synthesized for consumption
283 **Figure 4G**. One explanation for this is that the elongation rate decreases in poorer growth conditions.
284 Cells, however, are still able to maintain a relatively high elongation rate even in stationary phase
285 ($\approx 8 \text{ aa/s}$, (*Dai et al., 2016, 2018*)). A second explanation is that there are mechanisms to regulate
286 biological activity in conditions of stress and nutrient-limitation; in particular through the small-
287 molecule alarmones (p)ppGpp (*Harris and Theriot, 2018*). Here we explore these two observations
288 to better understand their consequence on growth rate.

289 We consider slow growth conditions (λ less than 0.5 hr^{-1}) by assuming that the decrease in
290 elongation rate is due to a limiting supply of amino acids and a need for the cell to maintain excess
291 nutrients for cellular homeostasis under steady-state growth. There is some experimental support
292 showing that in poorer nutrient growth conditions, cells have lower amino acids concentrations
293 (*Bennett et al., 2009*). We proceed by coarse grainig the cell's amino acid supply as an single,
294 effective rate-limiting species (see Appendix XX for a more complete discussion). Under such a
295 scenario, the elongation rate can described as simply depending on the maximum elongation rate
296 ($\approx 17.1 \text{ aa/s}$, (*Dai et al., 2016, 2018*)), an effective K_d , and the limiting amino acid concentration
297 $[aa]_{eff}$. Specifically, the elongation rate is given by,

$$r_t = r_t^{max} \cdot \frac{1}{1 + K_d/[aa]_{eff}}. \quad (3)$$

298 For cells growing in minimal media + glucose, the amino acid concentration is of order 100 mM
299 (BNID: 110093, (*Milo et al., 2010; Bennett et al., 2009*)). With a growth rate of about 0.6 hr^{-1} and
300 elongation rate of 12.5 aa per second (*Dai et al., 2016*), we can estimate an effective K_d of about 40
301 mM. Ultimately the steady state amino acid concentration will depend on the difference between
302 the supply of amino acids r_{aa} and consumption by ribosomes $r_t \cdot R \cdot f_a$, where f_a accounts for the
303 possible reduction of actively translating ribosomes.

304 In **Figure 4E** we consider how the maximal growth rate and elongation rates vary as a function of
305 the number of actively translating ribosomes in this slow growth regime (see Supplemental Section
306 XX for a complete description of the model). If we consider $r_a a$ to be reflective of a specific growth
307 condition, by considering lines of constant $r_a a$, we find that cells grow fastest by maximizing their
308 fraction of actively translating ribosomes. When we consider the experimental measurements from
309 *Dai et al.*, we see that although cells indeed reduce $R \cdot f_a$, they do so in a way that keeps $[aa]_{eff}$
310 relatively constant. Given our estimate for the K_d of 40 mM, we would only expect a decrease from
311 100 mM to about 35 mM in the slowest growth conditions. While experimental data is limited, amino
312 acid concentrations only decrease to about 60 mM for cells grown in minimal media + acetate (λ
313 0.3 hr^{-1} in our proteomic data; value obtained from *Bennett et al. (2009)*), qualitatively consistent
314 with our expectations.

315 Given the quantitative data from *Dai et al.*, which determined f_a across the entire range of
316 growth rates across our data, we next estimated the active fraction of ribosomal protein. As shown
317 in **Figure 4(G)**, we find that cells grow at a rate near the expected translation maximum expected

318 from Equation 1, using the maximum elongation rate of $r_t = 17.1$ aa per second. This is in contrast
 319 to the reality that cells ribosomes are translating at almost half this rate in the poorest growth
 320 conditions. This suggests that there are alternative ways to grow according to the translated-limited
 321 growth rate. Even though *E. coli* cells do not scale their ribosomal content to zero, they appear to
 322 achieve the same end by regulating the fraction of their ribosomes in poorer nutrient conditions.

323 [NB, important to include in discussion section: A number of recent papers highlight the
 324 possibility that (p)ppGpp may even provide a causal explanation for the nutrient-limit scaling law. In
 325 the context of ribosomal activity, increased levels of (p)ppGpp is associated with lower ribosomal
 326 content, and at slow growth appear to reduce the fraction of actively translating ribosomes (*Dai*
 327 *et al., 2016, 2018*). Titration of the cellular (p)ppGpp concentrations (up or down) can invoke similar
 328 proteomic changes reminiscent of those observed under nutrient limitation (*Zhu and Dai, 2019*). In
 329 light of the limiting dependence of ribosome copy number on chromosomal content, it was recently
 330 shown that growth (p)ppGpp null strain abolished both the cell size scaling and changes to the $\langle \#$
 331 $\text{ori} \rangle / \langle \# \text{ter} \rangle$ ratio. Rather, cells exhibited a $\langle \# \text{ori} \rangle / \langle \# \text{ter} \rangle$ closer to 4 and cell size more consistent
 332 with a fast growth state where (p)ppGpp levels are low (*Fernández-Coll et al., 2020*.)]

333 References

- 334 Aidelberg, G., Towbin, B. D., Rothschild, D., Dekel, E., Bren, A., and Alon, U. (2014). Hierarchy of non-glucose
 335 sugars in Escherichia coli. *BMC Systems Biology*, 8(1):133.
- 336 Antonenko, Y. N., Pohl, P., and Denisov, G. A. (1997). Permeation of ammonia across bilayer lipid membranes
 337 studied by ammonium ion selective microelectrodes. *Biophysical Journal*, 72(5):2187–2195.
- 338 Assentoft, M., Kaptan, S., Schneider, H.-P., Deitmer, J. W., de Groot, B. L., and MacAulay, N. (2016). Aquaporin 4
 339 as a NH₃ Channel. *Journal of Biological Chemistry*, 291(36):19184–19195.
- 340 Bauer, S. and Ziv, E. (1976). Dense growth of aerobic bacteria in a bench-scale fermentor. *Biotechnology and*
 341 *Bioengineering*, 18(1):81–94. _eprint: <https://onlinelibrary.wiley.com/doi/10.1002/bit.260180107>.
- 342 Belliveau, N. M., Barnes, S. L., Ireland, W. T., Jones, D. L., Sweredoski, M. J., Moradian, A., Hess, S., Kinney, J. B., and
 343 Phillips, R. (2018). Systematic approach for dissecting the molecular mechanisms of transcriptional regulation
 344 in bacteria. *Proceedings of the National Academy of Sciences*, 115(21):E4796–E4805.
- 345 Bennett, B. D., Kimball, E. H., Gao, M., Osterhout, R., Van Dien, S. J., and Rabinowitz, J. D. (2009). Absolute
 346 metabolite concentrations and implied enzyme active site occupancy in Escherichia coli. *Nature Chemical*
 347 *Biology*, 5(8):593–599.
- 348 Booth, I. R., Mitchell, W. J., and Hamilton, W. A. (1979). Quantitative analysis of proton-linked transport systems.
 349 The lactose permease of Escherichia coli. *Biochemical Journal*, 182(3):687–696.
- 350 Dai, X., Zhu, M., Warren, M., Balakrishnan, R., Okano, H., Williamson, J. R., Fredrick, K., and Hwa, T. (2018). Slowdown of Translational Elongation in Escherichia coli under Hyperosmotic Stress. - PubMed - NCBI. *mBio*, 9(1):281.
- 353 Dai, X., Zhu, M., Warren, M., Balakrishnan, R., Patsalo, V., Okano, H., Williamson, J. R., Fredrick, K., Wang, Y.-P., and Hwa, T. (2016). Reduction of translating ribosomes enables Escherichia coli to maintain elongation rates during slow growth. *Nature Microbiology*, 2(2):16231.
- 356 Escalante, A., Salinas Cervantes, A., Gosset, G., and Bolívar, F. (2012). Current knowledge of the Escherichia coli
 357 phosphoenolpyruvate-carbohydrate phosphotransferase system: Peculiarities of regulation and impact on
 358 growth and product formation. *Applied Microbiology and Biotechnology*, 94(6):1483–1494.
- 359 Feist, A. M., Henry, C. S., Reed, J. L., Krummenacker, M., Joyce, A. R., Karp, P. D., Broadbelt, L. J., Hatzimanikatis, V., and Palsson, B. Ø. (2007). A genome-scale metabolic reconstruction for Escherichia coli K-12 MG1655 that accounts for 1260 ORFs and thermodynamic information. *Molecular Systems Biology*, 3(1):121.
- 362 Fernández-Coll, L., Maciąg-Dorszynska, M., Tailor, K., Vadia, S., Levin, P. A., Szalewska-Palasz, A., Cashel, M., and
 363 Dunny, G. M. (2020). The Absence of (p)ppGpp Renders Initiation of Escherichia coli Chromosomal DNA
 364 Synthesis Independent of Growth Rates. *mBio*, 11(2):45.

- 365 Gama-Castro, S., Salgado, H., Santos-Zavaleta, A., Ledezma-Tejeida, D., Muñiz-Rascado, L., García-Sotelo, J. S.,
 366 Alquicira-Hernández, K., Martínez-Flores, I., Pannier, L., Castro-Mondragón, J. A., Medina-Rivera, A., Solano-Lira,
 367 H., Bonavides-Martínez, C., Pérez-Rueda, E., Alquicira-Hernández, S., Porrón-Sotelo, L., López-Fuentes, A.,
 368 Hernández-Koutoucheva, A., Moral-Chávez, V. D., Rinaldi, F., and Collado-Vides, J. (2016). RegulonDB version
 369 9.0: High-level integration of gene regulation, coexpression, motif clustering and beyond. *Nucleic Acids
 370 Research*, 44(D1):D133–D143.
- 371 Harris, L. K. and Theriot, J. A. (2018). Surface Area to Volume Ratio: A Natural Variable for Bacterial Morphogenesis.
 372 *Trends in microbiology*, 26(10):815–832.
- 373 Harris, R. M., Webb, D. C., Howitt, S. M., and Cox, G. B. (2001). Characterization of PitA and PitB from *Escherichia
 374 coli*. *Journal of Bacteriology*, 183(17):5008–5014.
- 375 Heldal, M., Norland, S., and Tumyr, O. (1985). X-ray microanalytic method for measurement of dry matter and
 376 elemental content of individual bacteria. *Applied and Environmental Microbiology*, 50(5):1251–1257.
- 377 Hui, S., Silverman, J. M., Chen, S. S., Erickson, D. W., Basan, M., Wang, J., Hwa, T., and Williamson, J. R. (2015).
 378 Quantitative proteomic analysis reveals a simple strategy of global resource allocation in bacteria. *Molecular
 379 Systems Biology*, 11(2):e784–e784.
- 380 Ireland, W. T., Beeler, S. M., Flores-Bautista, E., Belliveau, N. M., Sweredoski, M. J., Moradian, A., Kinney, J. B., and
 381 Phillips, R. (2020). Deciphering the regulatory genome of *Escherichia coli*, one hundred promoters at a time.
 382 *bioRxiv*.
- 383 Jacob, F. and Monod, J. (1961). Genetic regulatory mechanisms in the synthesis of proteins. *Journal of Molecular
 384 Biology*, 3(3):318–356.
- 385 Jun, S., Si, F., Pugatch, R., and Scott, M. (2018). Fundamental principles in bacterial physiology - history, recent
 386 progress, and the future with focus on cell size control: A review. *Reports on Progress in Physics*, 81(5):056601.
- 387 Khademi, S., O'Connell, J., Remis, J., Robles-Colmenares, Y., Miercke, L. J. W., and Stroud, R. M. (2004). Mechanism
 388 of Ammonia Transport by Amt/MEP/Rh: Structure of AmtB at 1.35 Å. *Science*, 305(5690):1587–1594.
- 389 Li, G.-W., Burkhardt, D., Gross, C., and Weissman, J. S. (2014). Quantifying absolute protein synthesis rates
 390 reveals principles underlying allocation of cellular resources. *Cell*, 157(3):624–635.
- 391 Liebermeister, W., Noor, E., Flamholz, A., Davidi, D., Bernhardt, J., and Milo, R. (2014). Visual account of protein
 392 investment in cellular functions. *Proceedings of the National Academy of Sciences*, 111(23):8488–8493.
- 393 Liu, M., Durfee, T., Cabrera, J. E., Zhao, K., Jin, D. J., and Blattner, F. R. (2005). Global Transcriptional Programs
 394 Reveal a Carbon Source Foraging Strategy by *Escherichia coli*. *Journal of Biological Chemistry*, 280(16):15921–
 395 15927.
- 396 Maaløe, O. (1979). *Regulation of the Protein-Synthesizing Machinery—Ribosomes, tRNA, Factors, and So On. Gene
 397 Expression*. Springer.
- 398 Milo, R., Jorgensen, P., Moran, U., Weber, G., and Springer, M. (2010). BioNumbers—the database of key numbers
 399 in molecular and cell biology. *Nucleic Acids Research*, 38(suppl_1):D750–D753.
- 400 Monod, J. (1947). The phenomenon of enzymatic adaptation and its bearings on problems of genetics and
 401 cellular differentiation. *Growth Symposium*, 9:223–289.
- 402 Neidhardt, F. C., Ingraham, J., and Schaechter, M. (1991). *Physiology of the Bacterial Cell - A Molecular Approach*,
 403 volume 1. Elsevier.
- 404 Peebo, K., Valgepea, K., Maser, A., Nahku, R., Adamberg, K., and Vilu, R. (2015). Proteome reallocation in
 405 *Escherichia coli* with increasing specific growth rate. *Molecular BioSystems*, 11(4):1184–1193.
- 406 Phillips, R. (2018). Membranes by the Numbers. In *Physics of Biological Membranes*, pages 73–105. Springer,
 407 Cham, Cham.
- 408 Ramos, S. and Kaback, H. R. (1977). The relation between the electrochemical proton gradient and active
 409 transport in *Escherichia coli* membrane vesicles. *Biochemistry*, 16(5):854–859.
- 410 Rosenberg, H., Gerdes, R. G., and Chegwidden, K. (1977). Two systems for the uptake of phosphate in *Escherichia
 411 coli*. *Journal of Bacteriology*, 131(2):505–511.

- 412 Schaechter, M., Maaløe, O., and Kjeldgaard, N. O. (1958). Dependency on Medium and Temperature of Cell Size
413 and Chemical Composition during Balanced Growth of *Salmonella typhimurium*. *Microbiology*, 19(3):592–606.
- 414 Schmidt, A., Kochanowski, K., Vedelaar, S., Ahrné, E., Volkmer, B., Callipo, L., Knoops, K., Bauer, M., Aebersold,
415 R., and Heinemann, M. (2016). The quantitative and condition-dependent *Escherichia coli* proteome. *Nature Biotechnology*, 34(1):104–110.
- 416
- 417 Scholz, S. A., Diao, R., Wolfe, M. B., Fivenson, E. M., Lin, X. N., and Freddolino, P. L. (2019). High-Resolution
418 Mapping of the *Escherichia coli* Chromosome Reveals Positions of High and Low Transcription. *Cell Systems*,
419 8(3):212–225.e9.
- 420 Scott, M., Gunderson, C. W., Mateescu, E. M., Zhang, Z., and Hwa, T. (2010). Interdependence of cell growth and
421 gene expression: origins and consequences. *Science*, 330(6007):1099–1102.
- 422 Sekowska, A., Kung, H.-F., and Danchin, A. (2000). Sulfur Metabolism in *Escherichia coli* and Related Bacteria:
423 Facts and Fiction. *Journal of Molecular Microbiology and Biotechnology*, 2(2):34.
- 424 Si, F., Le Treut, G., Sauls, J. T., Vadia, S., Levin, P. A., and Jun, S. (2019). Mechanistic Origin of Cell-Size Control and
425 Homeostasis in Bacteria. *Current Biology*, 29(11):1760–1770.e7.
- 426 Si, F., Li, D., Cox, S. E., Sauls, J. T., Azizi, O., Sou, C., Schwartz, A. B., Erickstad, M. J., Jun, Y., Li, X., and Jun, S. (2017).
427 Invariance of Initiation Mass and Predictability of Cell Size in *Escherichia coli*. *Current Biology*, 27(9):1278–1287.
- 428 Sirko, A., Zatyka, M., Sadowy, E., and Hulanicka, D. (1995). Sulfate and thiosulfate transport in *Escherichia coli*
429 K-12: Evidence for a functional overlapping of sulfate- and thiosulfate-binding proteins. *Journal of Bacteriology*,
430 177(14):4134–4136.
- 431 Stasi, R., Neves, H. I., and Spira, B. (2019). Phosphate uptake by the phosphonate transport system PhnCDE.
432 *BMC Microbiology*, 19.
- 433 Szenk, M., Dill, K. A., and de Graff, A. M. R. (2017). Why Do Fast-Growing Bacteria Enter Overflow Metabolism?
434 Testing the Membrane Real Estate Hypothesis. *Cell Systems*, 5(2):95–104.
- 435 Taheri-Araghi, S., Bradde, S., Sauls, J. T., Hill, N. S., Levin, P. A., Paulsson, J., Vergassola, M., and Jun, S. (2015).
436 Cell-size control and homeostasis in bacteria. - PubMed - NCBI. *Current Biology*, 25(3):385–391.
- 437 Taymaz-Nikerel, H., Borujeni, A. E., Verheijen, P. J. T., Heijnen, J. J., and van Gulik, W. M.
438 (2010). Genome-derived minimal metabolic models for *Escherichia coli* MG1655 with estimated
439 in vivo respiratory ATP stoichiometry. *Biotechnology and Bioengineering*, 107(2):369–381. _eprint:
440 <https://onlinelibrary.wiley.com/doi/pdf/10.1002/bit.22802>.
- 441 Valgepea, K., Adamberg, K., Seiman, A., and Vilu, R. (2013). *Escherichia coli* achieves faster growth by increasing
442 catalytic and translation rates of proteins. *Molecular BioSystems*, 9(9):2344.
- 443 van Heeswijk, W. C., Westerhoff, H. V., and Boogerd, F. C. (2013). Nitrogen Assimilation in *Escherichia coli*: Putting
444 Molecular Data into a Systems Perspective. *Microbiology and Molecular Biology Reviews*, 77(4):628–695.
- 445 Willsky, G. R., Bennett, R. L., and Malamy, M. H. (1973). Inorganic Phosphate Transport in *Escherichia coli*:
446 Involvement of Two Genes Which Play a Role in Alkaline Phosphatase Regulation. *Journal of Bacteriology*,
447 113(2):529–539.
- 448 Zhang, L., Jiang, W., Nan, J., Almqvist, J., and Huang, Y. (2014a). The *Escherichia coli* CysZ is a pH dependent
449 sulfate transporter that can be inhibited by sulfite. *Biochimica et Biophysica Acta (BBA) - Biomembranes*,
450 1838(7):1809–1816.
- 451 Zhang, Z., Aboulwafa, M., and Saier, M. H. (2014b). Regulation of crp gene expression by the catabolite
452 repressor/activator, cra, in *Escherichia coli*. *Journal of Molecular Microbiology and Biotechnology*, 24(3):135–141.
- 453 Zhu, M. and Dai, X. (2019). Growth suppression by altered (p)ppGpp levels results from non-optimal resource
454 allocation in *Escherichia coli*. *Nucleic Acids Research*, 47(9):4684–4693.